ELSEVIER

Chemical Engineering Journal 75 (1999) 31–46

Chemical Engineering Journal

Optimization and non-linear control of a batch emulsion polymerization reactor

C. Gentric, F. Pla, M.A. Latifi, J.P. Corriou*

Laboratoire des Sciences du Génie Chimique UPR 6811 CNRS-ENSIC-INPL, 1 Rue Grandville, BP 451, 54001, Nancy Cedex, France

Abstract

The optimal temperature policy which minimizes the terminal time in a batch emulsion polymerization reactor of styrene and α-methylstyrene was determined by means of orthogonal collocation techniques combined with a general non-linear programming method. The constraints concern the final latex properties and the thermal limitations of the pilot plant. An experimental validation has been realized. The optimal temperature profile was tracked using a non-linear geometric control technique which is particularly adapted to polymerization reactor control. An extended Kalman filter was used to estimate the non-measured state variables. Experimental results showed excellent agreement with predictions for this complex system. A good temperature tracking was observed and the product quality was well predicted and controlled. © 1999 Elsevier Science S.A. All rights reserved.

Keywords: Optimization; Non-linear control; Polymerization reactors

1. Introduction

Important objectives in polymer production plants, as in any chemical industry, are:

improvement of safety (safe and stable operation), quality and productivity,
minimum cost operation (energy conservation, manpower reduction, ...),
satisfying environmental conditions.

The optimization and control of polymerization reactors is therefore of great interest.

End-use properties of polymers (such as tensile strength, flexibility, elasticity, toughness...) are often related to their molecular characteristics which strongly depend on the reactor operating conditions (temperature, monomer or initiator concentration, initiator type, mixing rate, heating–cooling fluid flowrate, feeding method of different components in the case of semi-batch processes, ...). The operating conditions also influence the reaction time.

An optimization problem for a polymerization reactor requires the definition of an objective function and the specification of constraints which are usually expressed in terms of reaction time and/or molecular characteristics. Great attention must also be paid to the industrial plants capacities and suitable constraints must be subsequently added to the optimization problem.

A large number of contributions, dealing with the optimization of batch polymerization reactors, can be found in the literature (see [1] for a review). Most papers concern homogeneous reactions. The objectives frequently encountered are the following:

the minimization of the batch period [1–16],
the minimization of the molecular weight distribution [10,13,17–21],
quality control [22,23].

For the solution of these optimal control problems, various optimization methods have been employed:

Pontryagin's maximum principle [2–10,13,15,22],
Lagrange's multipliers [2,11,12,14],
multiobjective optimization technique [16],
orthogonal collocation with a successive quadratic programming method [1].

Experimental validation of the off-line computed optimal profiles was carried out in many of these studies [2–5,7,8,10–13,16,18,21].

Although the optimization of homogeneous polymerization reactors has been widely analyzed, only a limited number of studies have dealt with emulsion polymerization reactors.

*Corresponding author. E-mail: corriou@ensic.u-nancy.fr

1385-8947/99/$ – see front matter
PII: S1385-8947(98)00116-8

Jang and Yang [24] and Jang and Lin [25] studied the batch time minimization of a vinyl acetate emulsion polymerization reactor to achieve a desired final conversion. The manipulated variables were the feed rate of the initiator and/or the reactor temperature. Constraints were set on the reaction rate, on the total amount of added initiator and on the average number of long-chain branch points per polymer molecule [25]. The optimization method used was a modified approach of Biegler [26], called mixed integration collocation optimization.

Asua and co-workers [27–29] determined the minimum-time monomer addition policies for composition control of emulsion copolymerization in semi-batch reactors with no optimal control method. The reactor was initially charged with the less reactive monomer and the required amount of the most reactive monomer to initially form a copolymer with the desired composition. The remaining of the most reactive monomer was then fed to the reactor at a time-varying flowrate that ensured the formation of a copolymer with constant composition.

Finally, de la Cal et al. [30] determined off-line the optimal monomer addition policy to produce emulsion copolymers with a specified composition profile in minimum time.

This paper deals with an experimental study of the optimization and control of a batch emulsion copolymerization reactor of styrene and α-methylstyrene, which has been rarely studied in the literature [31–33]. First, the non-linear model of the reactor dynamics is briefly described. An optimal temperature profile is then determined off-line, taking into account the reactor productivity, the final product quality and operating constraints resulting from pilot plant limitations. The orthogonal collocation method combined with a non-linear programming method (i.e. sequential quadratic programming) is used to solve the dynamic optimization problem. This is a very appropriate approach allowing to treat all types of optimal control problems, and to deal effectively with any kind of constraints. A non-linear geometric controller coupled with an extended Kalman filter for state estimation is employed to track the optimal temperature profile. Finally, an experimental validation of the calculated optimal policies is carried out.

2. Process model

Despite its wide use, emulsion polymerization is a process difficult to model because of its complex kinetic mechanism. The main reason is the presence of several phases in the reaction mixture. The modeling of emulsion polymerization requires the description of complex physical and chemical phenomena arising from both polymer and colloid science.

Since the successful optimization and control of a polymer process depend strongly on the availability of a reliable model, this modeling step is very important. There exist several types of models, mainly depending on the purpose they are devised for. The classical approach of the macromolecular chemists is based on a detailed inventory of all physical phenomena and chemical reactions involved. It often leads to a large number of ordinary and partial differential equations with unknown parameters which sometimes cannot be determined through experiments. In the case of optimization and control, the reactor model should be detailed and precise enough (to predict the effect of the main process input variables on the process output variables, and to represent the complex relationship between operating conditions, kinetics, and final product properties). In addition, the model should contain parameters that can be determined from experimental measurements. The model should also remain at a complexity level allowing optimal profile determination and control law computation. Thus, a tendency model is the most appropriate.

The model developed here allows, with a limited number of assumptions and parameters, to describe the main phenomena involved: radical formation, particle nucleation, radical capture by micelles and particles, termination, propagation, transfer to monomer and heat transfer phenomena. The state variables considered are the monomer concentration, the number of particles per volume unit, the moments of the molecular weight distribution, the reactor and jacket temperatures.

2.1. Kinetic model

Four essential components are required to carry out an emulsion polymerization process: the dispersion medium which in general is water, the monomer which is often slightly soluble in water, the initiator which is water soluble, and an emulsifier.

The kinetics of an emulsion polymerization process is classically divided into three distinct periods called intervals I, II and III:

Interval I: Free radicals are produced in the aqueous phase by initiator decomposition. They are captured by the micelles swollen with monomer. The polymerization begins in these micelles. This interval corresponds to the particle nucleation (here, only the case of heterogeneous nucleation is presented) and stops when all the micelles have disappeared.
Interval II: Particles are growing. Monomer diffuses rapidly from monomer droplets towards the particles which are saturated with monomer as long as monomer droplets exist. This interval ceases when monomer droplets have disappeared.
Interval III: The monomer concentration in the particles decreases.

The model used in this paper is based on the following assumptions which are valid for our system:

Styrene and α-methylstyrene are both hydrophobic monomers, thus only micellar nucleation is taken into account.

Due to this hydrophobic character, propagation, transfer to monomer, termination reactions in the aqueous phase and radical desorption are neglected.

Termination in particles is considered to be very rapid compared to radical entry into particles, thus it can be assumed that there is no more than one radical per polymer particle (zero–one system) [34]. This allows to write that: $P_j^\bullet = N^\bullet$.

The considered maximum conversion is generally around 65% so that the gel effect has not occurred yet [35] and thus is not included in the model to avoid unnecessary complexity.

The kinetic mechanism is then written:

Initiator decomposition:

$$A \rightarrow 2R^\bullet; \quad R_a = 2fk_d A \tag{1}$$

Particle formation:

$$R^\bullet + m \rightarrow N^\bullet; \quad R_n = k_{cm} m R^\bullet \tag{2}$$

Radical entry into inactive particles:

$$N + R^\bullet \rightarrow N^\bullet; \quad R_i = k_{cp} N R^\bullet \tag{3}$$

Radical entry into active particles:

$$N^\bullet + R^\bullet \rightarrow N; \quad R_t = k_{cp} N^\bullet R^\bullet \tag{4}$$

Propagation:

$$P_j^\bullet + M \rightarrow P_{j+1}^\bullet; \quad R_p = k_p M_p P_j^\bullet = k_p M_p N^\bullet \tag{5}$$

Transfer to monomer:

$$P_j^\bullet + M \rightarrow M^\bullet + P_j; \quad R_{trM} = k_{trM} M_p P_j^\bullet = k_{trM} M_p N^\bullet \tag{6}$$

The rate of particle formation can be derived from this mechanism. The quasi-steady-state approximation allows to determine the initiator radical concentration in the water phase:

$$R^\bullet = \frac{R_a}{k_{cm} m + k_{cp} N_p} \tag{7}$$

The total number of particles is deduced from Eq. (7) and from the rate of radical entry into micelles Eq. (2):

$$\frac{dN_p}{dt} = k_{cm} m \frac{R_a N_a}{k_{cm} m + k_{cp} N_p} \tag{8}$$

In the same way as Harada et al. [36] who studied the styrene emulsion homopolymerization, we introduce a capturing efficiency of the particles with respect to the micelles:

$$\varepsilon = \frac{k_{cp} n_s}{k_{cm}} \tag{9}$$

where n_s is the aggregation number of a micelle defined as

$$n_s = \frac{S N_a}{m} \tag{10}$$

Thus, during step 1

$$\frac{dN_p}{dt} = \frac{R_a N_a}{1 + (\varepsilon N_p / S N_a)} \tag{11}$$

where, with the classical assumption that emulsifier molecules are adsorbed in monomolecular layers at the polymer particles surface

$$S = S_0 - k_v (X M_0)^{2/3} N_p^{1/3} \tag{12}$$

with

$$k_v = \left(\frac{36\pi M_M^2}{\omega_p^2 \rho_p^2 (a_s N_a)^3} \right)^{1/3} \tag{13}$$

where X is the conversion and M_o the overall initial monomer concentration.

The rate of monomer consumption is classically expressed as

$$\frac{dM}{dt} = -R_p = -k_p M_p \frac{N_p}{N_a} \bar{n} \tag{14}$$

Here, since the objective is temperature control, only the overall monomer concentration is described. Castellanos [33] studied the copolymerization of styrene and α-methylstyrene at three temperatures (50°, 65° and 85°C) and four different initial monomer compositions (10%, 25%, 35% and 50% in mass of α-methylstyrene). He found experimentally that there was no composition change during the polymerization under these conditions and showed that the global propagation constant could be written as

$$k_p = k_{psty} \exp(a f_{MS}) \tag{15}$$

where k_{psty} is the styrene homopolymerization propagation rate constant, a is a constant, f_{MS} is the initial α-methylstyrene mole fraction.

The monomer concentration in the particles M_p corresponds to the particle saturation during steps 1 and 2, and then decreases with conversion during step 3

$$M_p = M_{pc} = \frac{(1 - X_c)\rho_M}{[(1 - X_c) + X_c \rho_M / \rho_P] M_M} \quad X \leq X_c, \text{ steps 1 and 2} \tag{16}$$

$$M_p = \frac{(1 - X)\rho_M}{[(1 - X) + X \rho_M / \rho_P] M_M} \quad X > X_c, \text{ step 3} \tag{17}$$

Rudin and Samanta [31] showed experimentally that $\bar{n}$ is equal to 0.5 for the styrene/α-methylstyrene copolymerization. Castellanos [33] confirmed this value, even at high conversions.

2.2. Molecular weight distribution model

The classical approach to describe the molecular weight distribution leads to balances for every macroradical or macromolecule taken individually. This detailed approach allows to determine the complete molecular weight distri-

bution. However, when complex phenomena are involved, this approach cannot be useful. The tendency model developed by Villermaux et al. [37] is also based on the classical kinetic scheme but all macroradicals and all macromolecules are considered globally, and their polymerization degree is not needed. The considered species are the global radical concentration, the global macromolecule concentration and the moments of the polymerization degrees.

Here, macromolecules are formed by the entry of an initiator radical into a particle already containing a macroradical (since termination is then quasi-instantaneous) or by transfer to monomer. These macromolecules have the same distribution as the macroradicals which are simply deactivated, thus

$$\frac{dP}{dt} = \frac{dQ_0}{dt} = \frac{d\mu_0 P}{dt} = R_t + R_{trM} \tag{18}$$

$$\frac{dQ_1}{dt} = \frac{d\mu_1 P}{dt} = L(R_t + R_{trM}) = R_p \tag{19}$$

$$\frac{dQ_2}{dt} = \frac{d\mu_2 P}{dt} = 2L^2(R_t + R_{trM}) \tag{20}$$

where

$$R_t = \frac{R_a \overline{n} N_p}{N_p + (S/\varepsilon)} \tag{21}$$

$$R_{trM} = k_{trM} M_p \frac{N_p}{N_a} \overline{n} \tag{22}$$

and

$$L = \frac{R_p}{R_t + R_{trM}} \tag{23}$$

The integration of these ordinary differential equations (ODE) provides the number and weight average molecular weights, and the polydispersity index:

$$\overline{M}_n = M_M \frac{Q_1}{Q_0}; \quad \overline{M}_w = M_M \frac{Q_2}{Q_1}; \quad I_p = \frac{\overline{M}_w}{\overline{M}_n} \tag{24}$$

Remark: The transfer to monomer rate constant is computed in a similar way as the propagation rate constant. Since there is no composition change during this copolymerization in the considered conditions, a global constant is thus considered.

2.3. Reactor dynamics model

The reaction takes place in a glass stirred tank batch reactor. Reactor temperature control is achieved by means of a cooling fluid flowing through a double jacket. This latter is itself considered at a mean single temperature T_j because of large constant coolant flowrate. The cooling fluid inlet temperature is controlled. Energy balances lead to the following ODE, describing the batch reactor and jacket temperature dynamics:

$$\frac{dT}{dt} = -\frac{V\Delta H}{m_r C_p} R_p + \frac{UA}{m_r C_p}(T_j - T) \tag{25}$$

Table 1
Values of the kinetic rate constants used in the model

Variable	Value	Unit
Initiator decomposition	$k_{do} = 4.5\times10^{16}$	s^{-1}
rate constants	$E_d = 140.2\times10^3$	J mol^{-1}
Initiator efficiency	$f = 0.5$	
Propagation	$k_{po} = 1.1\times10^7$	l mol^{-1} s^{-1}
rate constants	$E_p = 29\times10^3$	J mol^{-1}
	$a = -7.3$	
Average number of radicals per particle	$\overline{n} = 0.5$	
Monomer concentration at saturation	$M_{pc} = 5.38$	mol l^{-1}
Area occupied by 1 g of emulsifier	$a_s = 1.8\times10^5$	dm^2 g^{-1}
Epsilon	$\varepsilon = 5\times10^{-16}$	g $part^{-1}$
Transfer to monomer	$k_{trMo} = 22\times10^{10}$	l mol^{-1} s^{-1}
rate constants	$E_{trM} = 85\times10^3$	J mol^{-1}
	$b = -4$	

$$\frac{dT_j}{dt} = \frac{F_j}{V_j}(T_{jin} - T_j) - \frac{UA}{\rho_j V_j C_j}(T_j - T) \tag{26}$$

The kinetic constants of the model are given in Table 1.

3. Optimal temperature profile

3.1. Problem statement

The aim of the present work is to maximize the productivity of an emulsion polymerization reactor, i.e. to minimize the batch period. Temperature which highly influences the rate of a polymerization process will be chosen as the control variable. A temperature increase accelerates the polymerization process, but also modifies some properties of the polymer. These properties can be described in terms of molecular characteristics: number average molecular weight, weight average molecular weight, polydispersity index.

The performance index will be then the final time, whereas the terminal constraints will allow to set the desired polymer properties: here they are defined as the final conversion (characterizing the polymer quantity which has been produced) and number average molecular weight.

The problem can be then expressed as follows

$$T^*(t) = \arg\{\min_{T(t)} J\} \tag{27}$$

where

$$J = t_f$$

subjected to

$$\frac{dx_i}{dt} = f_i(x, T, t),\ i = 1, \ldots, 5 \quad \text{state model}$$

$$x_1(t_0) = M_0$$

$$x_i(t_0) = 0,\ i = 2, \ldots, 5 \quad \text{initial conditions}$$

$$1 - \frac{x_1(t_f)}{M_0} = X_f \quad \text{final conversion}$$

$$M_M \frac{x_4(t_f)}{x_3(t_f)} = \overline{M}_{nf} \quad \text{final number average molecular weight}$$

The state-vector is only formed by the global monomer concentration, the number of particles, and the moments of the molecular weight distribution: $x = (M, N_p, Q_0, Q_1, Q_2)$. Presently, the reactor temperature dynamics is ignored because at this stage the objective is to determine an optimal reactor temperature profile.

3.2. Optimization method

The optimization problem Eq. (27) can be written again in a more general form:

$$(u, q)^* = \arg\{\min_{u(t),q} J\} \tag{28}$$

where

$$J = \Psi[x(t_f), q, t_f] + \int_{t_0}^{t_f} \Phi[x(t), u(t), q, t]\mathrm{d}t$$

subjected to

$g[x(t), u(t), q, t] \leq 0$ instantaneous inequality constraints

$h[x(t), u(t), q, t] = 0$ instantaneous equality constraints

$\dot{x}(t) = f[x(t), u(t), q, t]$ state model

$x(t_0) = x_0$ initial conditions

$x_{inf} \leq x(t) \leq x_{sup}$

$u_{inf} \leq u(t) \leq u_{sup}$

$q_{inf} \leq q \leq q_{sup}$

where u is the control variables vector, q is the control parameters vector, J is the performance criterion.

The solution of optimization problems involving both algebraic and differential equations has been recently developed [1,26,38–41]. The basic idea is to transform the initial problem into an approximated problem. Two main approaches can be used.

In the first one, only the control variables are parameterized by means of zeroth or higher order spline functions. The system of differential equations is solved with this parameterization. The parameters, i.e. control variables, are then adjusted with a non-linear programming algorithm in an outer loop. This technique was developed by Goh and Teo [41] and applied to a fed-batch fermentation process by Chen and Hwang [42]. These methods can be computationally time consuming because they require the integration of the differential equation system at each iteration and may be slowly converging.

In the second approach, both control and state variables are parameterized. This method was first described in the 1970s (Neuman and Sen [43], Tsang et al. [44]), but has not been extensively used because it led to too large non-linear programming problems. The development of recent non-linear programming methods made this approach more attractive [1,26,38,45,46]. According to this method, polynomial approximation and orthogonal collocation are used to convert the initial problem to a non-linear programming problem. The optimization parameters are then the polynomials coefficients. This interesting technique allows to treat every kind of optimal control problem. It is also easy to implement, rapid and leads to simultaneous integration and optimization. The main drawbacks of this technique are the expansion of the problem size and the infeasibility path type method. Biegler [26] demonstrated on a small example the superiority of this method over other classical techniques: Control Vector Iteration (a numerical method to solve the maximum principle) and Control Vector Parameterization (which consists in approximating the control variables and belongs to the first aforementioned approach). This technique was applied to a catalytic CSTR [39], to a fed-batch fermentor [45], and to batch polymerization reactors [1].

3.2.1. Orthogonal collocation

Since emulsion polymerization kinetics are different in the three steps, i.e. intervals, I, II, and III, the optimal control profile may not be continuous [25]. In this case, orthogonal collocation on finite elements was used [38]. Each finite element $\Delta\alpha_i$ is bounded by two knots: α_i and α_{i+1}. On these finite elements, the control and state variables are approximated by Lagrange polynomials of respective orders NC and NC−1:

$$x^i_{NC}(\tau) = \sum_{j=0}^{NC} a_{ij}\Phi_{ij}(\tau); \quad \Phi_{ij}(\tau) = \prod_{k=0,\neq j}^{NC}\left(\frac{\tau - \tau_{ik}}{\tau_{ij} - \tau_{ik}}\right) \tag{29}$$

$$u^i_{NC-1}(\tau) = \sum_{j=1}^{NC} b_{ij}\Psi_{ij}(\tau); \quad \Psi_{ij}(\tau) = \prod_{k=1,\neq j}^{NC}\left(\frac{\tau - \tau_{ik}}{\tau_{ij} - \tau_{ik}}\right) \tag{30}$$

for i=1,. . ., NE.

The dimensionless time, τ, allows to treat easily free end-time problems.

NE is the considered number of finite elements.

The τ_{ij}'s are defined as

$$\tau_{ij} = \alpha_i + \gamma_j(\alpha_{i+1} - \alpha_i); \quad i = 1, \ldots, NE; \quad j = 0, \ldots, NC \tag{31}$$

where $\gamma_0 = 0$ and the γ_j's (j=1, . . ., NC) are the zeros of a Legendre polynomial defined on (0,1).

Replacing the state and control variables by their polynomial approximations in the state system leads to the following algebraic residual equations

$$r(\tau_{il}) = \sum_{j=0}^{NC} a_{ij}\dot{\Phi}_{ij}(\tau_{il}) - t_f.f[a_{il}, b_{il}, q, \tau_{il}] = 0;$$

$$l = 1, \ldots, NC; \quad i = 1, \ldots, NE \tag{32}$$

where

$$\dot{\Phi}_{ij}(\tau_{il}) = \frac{\dot{\Phi}_j(\tau_l)}{\Delta\alpha_i} \tag{33}$$

Then it is necessary to impose the continuity of the state variables between two successive finite elements and to bound the extrapolation of the control variables at both ends of the finite elements since they are only defined inside each element.

Finally the problem Eq. (28) can be approximated as follows

$$(a_{il}, b_{il}, q, \alpha_i, t_f)^* = \arg\{\min_{a_{il},b_{il},q,\alpha_i,t_f} J[a_{il}, b_{il}, q, t_f]\} \quad (34)$$

subjected to

$$g[a_{il}, b_{il}, q, \tau_{il}] \leq 0$$

$$h[a_{il}, b_{il}, q, \tau_{il}] = 0$$

$$r(\tau_{il}) = 0$$

$$a_{10} = x_0$$

$$a_{i0} = \sum_{j=0}^{NC} a_{i-1j}\Phi_j(\tau = 1)$$

$$u_{inf} \leq u^i_{NC-1}(\alpha_i) \leq u_{sup}$$

$$u_{inf} \leq u^i_{NC-1}(\alpha_{i+1}) \leq u_{sup}$$

$$x_{inf} \leq a_{il} \leq x_{sup}$$

$$u_{inf} \leq b_{il} \leq u_{sup}$$

$$q_{inf} \leq q \leq q_{sup}$$

The optimization problem parameters are the state and control variables values at the collocation points defined by Eq. (31), the final time, and the position of the knots, which correspond at convergence to the control variables discontinuities. The state and control variables are then completely defined by Eqs. (29) and (30). This method allows to handle easily all types of constraints.

3.2.2. Non-linear programming method

The resulting non-linear problem Eq. (34) can then be solved using a successive quadratic programming technique. Here we used the NLPQL software developed by Schittkowski (NLPQL, version 2.4, June 1991) (see [47] for more details).

3.3. Optimization results

The results presented here correspond to an initial α-methylstyrene fraction f_{MS} of 10%. The lower and upper temperature constraints are 313 and 343 K, respectively. A temperature greater than 313 K will ensure a sufficient reaction rate, and 343 K is the maximum temperature allowed by our pilot plant. The number of finite elements, NE, was set equal to 3, corresponding to the three steps of the emulsion polymerization kinetics. A value of two or three finite elements modifies very little the optimal profile, thus three elements were maintained in order to have a larger number of collocation points. The state variables are of very different magnitude orders: concentrations, number of particles per volume unit, moments of the molecular weight distribution, temperature, reaction time. Therefore the variables were normalized as follows:

$$x_{1n} = x_1$$

$$x_{2n} = x_2/10^{17}$$

$$x_{3n} = x_3/10^{-4}$$

$$x_{4n} = x_4$$

$$x_{5n} = x_5/10^5$$

$$t_{fn} = t_f/10000$$

$$T_n = T/300$$

Two different cases have been studied: first, when no constraint on the reactor cooling rate is imposed, a sharp temperature gradient in the profile can then be theoretically achieved. Second, and more realistic, when the actual cooling rate of our pilot plant is introduced as a constraint, which results in a lower temperature gradient.

3.3.1. Unconstrained reactor cooling rate

The problem must be carefully initialized. In this case, the initialization corresponds to the integration of the state model at constant temperature. This temperature is chosen as the optimal temperature for an isothermal reaction and for the same constraints on X_f and $\overline{M}_{nf}$. The transitions between steps 1 and 2 (N_p becoming constant) and 2 and 3 ($X=X_c$) at this temperature will provide initial values for the position of the knots of the finite elements. The time at which the desired conversion X_f is reached will give an initial value for t_f. The position of the collocation points τ_{ij} is deduced from the values of the α_i's and t_f.

The number of collocation points NC is chosen large enough so that the interpolated state profiles and the a posteriori integration of the state system with a fifth-order Runge–Kutta method give the same results. In this case, a number of collocation points per finite element of 2 or 3 is sufficient. A greater value of NC does not significantly modify the optimal temperature profiles.

Fig. 1 shows the optimal temperature profiles for the case of a final conversion $X_f = 60\%$ and three different values of the final number average molecular weight, $\overline{M}_{nf}$: 1.5, 2 and 3×10^6 g mol^{-1}. The optimal profile corresponds to a temperature equal to the maximum temperature during the nucleation step (during this step, the constraint on the maximum temperature is active) and then a quasi-constant temperature depending on the final desired molecular weight. During interval I, the high temperature corresponds to the formation of a maximum number of particles and then leads to a reduction of the reaction time. Indeed, the polymerization rate is directly proportional to the number of particles. Then the constant temperature decreases when the desired molecular weight increases. The batch period is consequently longer when the desired molecular weight is higher, as shown in Table 2.

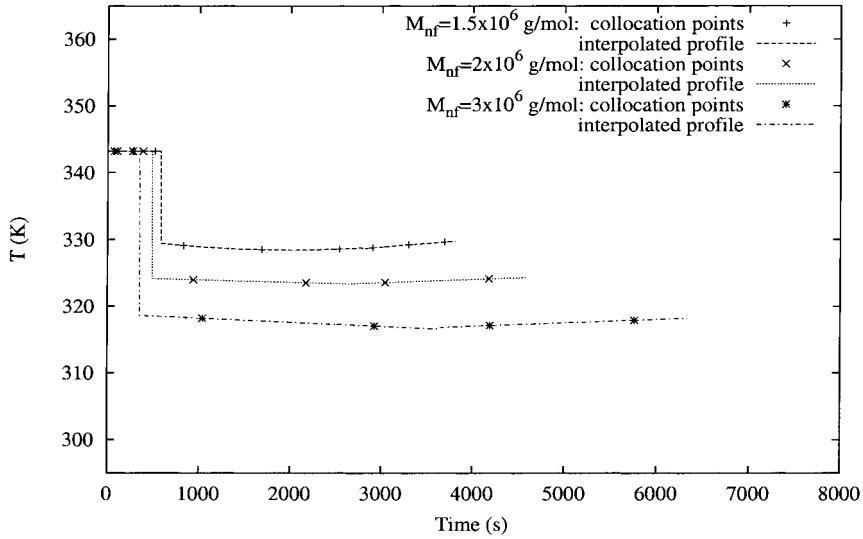

Fig. 1. Optimal temperature profiles for $X_f = 60\%$ and $M_{nf} = 1.5$, 2 and 3×10^6 g mol^{-1} (unconstrained cooling rate).

When different final constraints on the conversion are imposed, almost the same optimal temperature profile is obtained. Only the reaction time depends on the desired final conversion (6335, 7550, 9285 s for final conversions $X_f = 60\%$, 70%, 80%, respectively).

In each case, the position of the first knot, which is included in the optimization process, corresponds to the end of the nucleation step, i.e. to a number of particles which ceases to increase and becomes constant. On the other hand, the position of the second knot does not exactly correspond to a conversion equal to X_c. As a matter of fact, there is no important change in the temperature profile between intervals II and III as it can be observed. Anyway, three finite elements are kept because they allow better interpolation.

Table 2 summarizes the results for the three considered final number average molecular weights and conversions. In particular, the optimal batch reaction times t_f can be compared to those obtained for isothermal operations at a temperature leading to the same final conversion and number average molecular weight: t_f^{iso}. The optimal temperature profile allows to increase the production rate considerably compared to an isothermal operation (the batch time is theoretically reduced from 1/3 to 1/2 for the studied cases). But this temperature profile is not physically realistic because it implies an instantaneous temperature decrease at the end of the nucleation step.

3.3.2. Constrained reactor cooling rate

In order to compute a more realistic temperature profile, a constraint must be imposed on the reactor temperature time derivative. This constraint will correspond to the reactor maximum cooling rate. At each collocation point, a new type of constraint is imposed: the temperature time derivative must be lower in magnitude than the reactor maximum cooling rate R_{cmax}. Since these are negative values, this constraint is expressed as

$$\sum_{j=1}^{NC} b_{ij}\dot{\Psi}_{ij}(\tau_{il}) \geq t_f.R_{cmax}; \quad l = 1, \ldots, NC; \quad i = 1, \ldots, NE \tag{35}$$

This represents a new type of constraint in comparison with the problem Eq. (28), and the collocation method allows to handle it very easily.

Moreover, it is necessary to impose the continuity of the control variables at each finite element knot:

$$u^i_{NC-1}(\alpha_i) = u^{i-1}_{NC-1}(\alpha_i) \quad i = 2, \ldots, NE \tag{36}$$

The problem is initialized here with the results of the previous optimization. Compared to the case where finite

Table 2
Optimization results without constraint on the reactor cooling rate

X_f^s	$\overline{M}_{nf}^s 10^{-6}$(g mol^{-1})	T^*_{iso} (K)	t_f^{iso} (s)	t_f (s)	t_f/t_f^{iso}	X_f^c	$\overline{M}_{nf}^c 10^{-6}$ (g mol^{-1})
0.6	1.5	331.63	5643	3805	0.674	0.5969	1.49
0.6	2	327.65	7413	4595	0.620	0.5934	1.98
0.6	3	322.18	10839	6335	0.584	0.5953	2.96
0.7	3	321.89	13665	7550	0.552	0.6927	2.96
0.8	3	321.52	17220	9285	0.539	0.7885	2.97

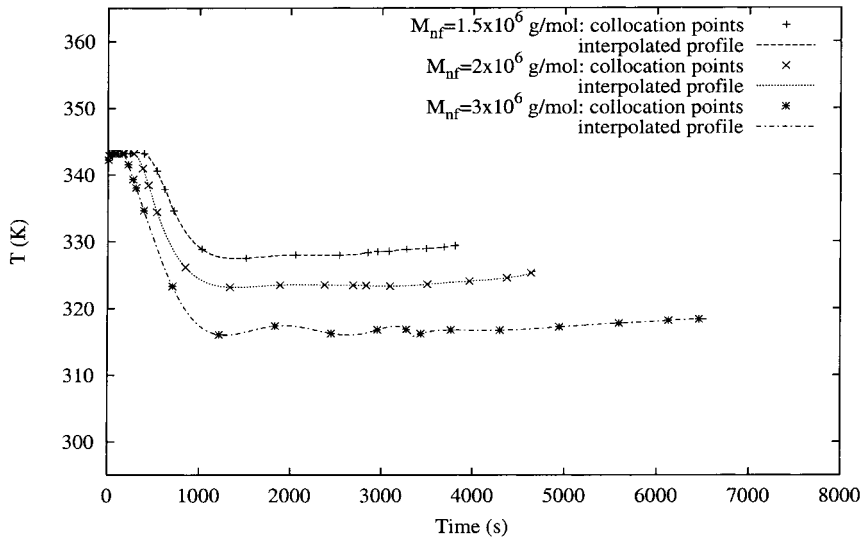

Fig. 2. Optimal temperature profiles for $X_f = 60\%$ and $M_{nf} = 1.5$, 2 and 3×10^6 g mol^{-1} (constrained cooling rate).

elements are not introduced, it is possible to compute control profiles with discontinuous first-order derivative at the knots.

As in the case of unconstrained reactor cooling rate, the number of collocation points is progressively increased in order to have a good agreement between interpolated and integrated state profiles. In this case, a number of collocation points per finite element of six or seven is sufficient.

Fig. 2 allows to compare the temperature profiles for the following final constraints: $X_f = 60\%$ and $\overline{M}_{nf} = 1.5$, 2 or 3×10^6 g mol^{-1} and a maximum reactor cooling rate of -0.04 K s^{-1}. The optimal temperature profile can be interpreted as follows: at the beginning the temperature is equal to the maximum allowed temperature, then decreases at the maximum cooling rate for the reactor, and finally becomes quasi-constant depending on the final desired number average molecular weight. As in the previous case, a maximum number of particles is formed at the beginning in order to reduce the batch time. But the maximum temperature cannot be maintained during all the nucleation step because of the constraint on the cooling rate. In fact, the temperature can no longer be reduced instantaneously at the end of interval I. During the second phase, the constraint on the temperature derivative is saturated. Lastly, as previously, the final temperature decreases when the desired final molecular weight increases and consequently the final time is greater when high molecular weight constraints are imposed (Table 3).

As in the unconstrained case, a change in the final constraint on X_f only modifies the final time but does not change the profile shape.

The position of the first knot still corresponds to the end of the nucleation step.

Table 3 summarizes the results for the three considered cases. The final time can be compared to the isothermal batch time leading to the same final polymer specifications. These batch periods are not much greater than those obtained with the non-realistic temperature profiles. Fig. 3 compares the conversion profiles for the isothermal case and the optimal temperature profile case, when the same constraints are imposed ($X_f = 60\%$ and $\overline{M}_{nf} = 2\times10^6$ g mol).

It is worth noticing that the optimized operation allows to improve the productivity, up to 40%, with respect to isothermal operation.

4. Non-linear geometric control and state estimation

The aim is now to control the reactor temperature in order to track the off-line determined temperature profile. A major characteristic of polymerization reactors is their complex non-linear behavior. This is especially the case for batch processes which are often employed for polymer production since they allow more flexibility. This particularity makes batch polymerization reactor control with classical linear

Table 3
Optimization results with constraint on the reactor cooling rate

X_f^s	$\overline{M}_{nf}^s$ 10^{-6} (g mol^{-1})	T_{iso}^* (K)	t_f^{iso} (s)	t_f (s)	t_f/t_f^{iso}	X_f^c	$\overline{M}_{nf}^c \times 10^{-6}$ (g mol^{-1})
0.6	1.5	331.63	5643	3846	0.682	0.5969	1.50
0.6	2	327.65	7413	4700	0.634	0.5924	2.03
0.6	3	322.18	10839	6541	0.603	0.5845	3.05

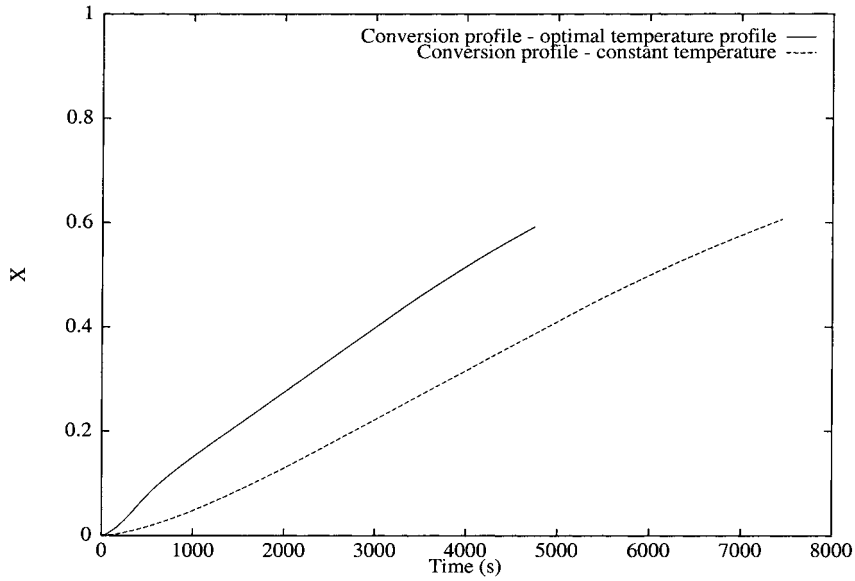

Fig. 3. Comparison between conversion profiles for $X_f = 60\%$ and $\overline{M}_{nf} = 2\times10^6$ g mol^{-1} corresponding to optimal constant and dynamic temperature profiles.

techniques very difficult. So there is a great interest in using non-linear control techniques. Non-linear control based on differential geometry has made great advances in the past 15 years [48] and has been successfully applied to chemical processes. The synthesis of the control law is based on the state model of the process and allows to take into account the system non-linearities. Non-linear control based on differential geometry has been applied already to polymerization reactors [49,50] but only few experimental studies have been realized so far [19].

Non-linear geometric control implies that all the state variables are known, but a problem with polymerization reactors is the lack of on-line measurements. Here we suppose that only the temperature is measurable, which is often the case in industrial practice. So a state observer is necessary to estimate the non-measurable state variables. Industrially, the Kalman filter is probably the most employed state observer. Here we use the extended Kalman filter [51] which is an extension of the classical linear Kalman filter to non-linear systems.

4.1. Non-linear geometric control through input/output linearization

Non-linear geometric control will be presented briefly. More details can be found in [48] and notations follow this classical textbook.

The control law is based on the state description of the system

$$\dot{x} = f(x) + g(x)u$$
$$y = h(x) \tag{37}$$

where x is the state vector, u is the input and y the output.

The necessary and sufficient condition for the input/output linearization to be possible is that the relative degree C of the system, defined as

$$L_g L_f^k h(x) = 0 \quad \forall k < r-1$$
$$L_g L_f^{r-1} h(x) \neq 0 \tag{38}$$

is finite. The notation $L_f^i h$ represents the ith Lie derivative of the function h along the vector field f.

Then the control law

$$u = \frac{-L_f^r h(x) + v}{L_g L_f^{r-1} h(x)} \tag{39}$$

gives the input–output linear response

$$y^{(r)} = v \tag{40}$$

where v is an external input.

A pole placement can be realized if the control law Eq. (39) is replaced by

$$u = \frac{-L_f^r h(x) - \sum_{i=0}^{r-1} c_i L_f^i h(x) + v}{L_g L_f^{r-1} h(x)} \tag{41}$$

where the c_i's are adjustable parameters chosen in order to realize the desired pole placement. Then the input–output response is

$$v = \sum_{i=0}^{r-1} c_i y^{(i)} + y^{(r)} \tag{42}$$

and an external PI controller can ensure the controller robustness

$$v = K_c \left[(y_{sp} - y) + 1/\tau_I \int_0^t (y_{sp} - y) \mathrm{d}t \right] \tag{43}$$

4.2. Extended Kalman filter

Since the model is continuous and the measurements are discrete, a Kalman filter in its continuous/discrete form is employed to estimate the states.

If the system is described by

$$\dot{x} = f(x,u,t) + w(t)$$
$$y_k = h(x(t_k),k) + v_k \quad (44)$$

where w and v_k are zero-mean white noises of covariance matrices Q and R, then the extended Kalman filter in its continuous/discrete form is defined by

prediction

state variables:

$$\frac{d\hat{x}^-}{dt} = f(\hat{x}^-,u,t) \quad (45)$$

covariance estimate:

$$\frac{dP^-}{dt} = FP^- + P^-F^T + Q \quad (46)$$

correction

Kalman gain

$$K_k = P_k^- H_k^T [H_k P_k^- H_k^T + R_k]^{-1} \quad (47)$$

state variable

$$\hat{x}_k^+ = \hat{x}_k^- + K_k[y_k - h(\hat{x}_k^-)] \quad (48)$$

covariance estimate

$$P_k^+ = (I - K_k H_k)P_k^- \quad (49)$$

where

$$F = \left.\frac{\partial f}{\partial x}\right|_{\hat{x}_k} \quad \text{and} \quad H = \left.\frac{\partial h}{\partial x}\right|_{\hat{x}_k^-}$$

4.3. Application to the batch emulsion polymerization reactor

4.3.1. Non-linear geometric control

Here the state vector is the following:

$$(x_1, x_2, x_3, x_4) = (M, N_p, T, T_j)$$

In fact, the moments of the molecular weight distribution have no influence on the reactor temperature, which is the variable to be controlled. The manipulated input is the jacket inlet temperature. The setpoint is the optimal reactor temperature profile computed in the previous part. The relative degree of the system calculated according to Eq. (38) is equal to 2. The control law coefficients are chosen so that the closed-loop response, of which the transfer function is:

$$\frac{Y(s)}{Y_{sp}(s)} = \frac{K_c(s + 1/\tau_I)}{s^3 + c_1 s^2 + (c_0 + K_c)s + K_c/\tau_I} \quad (50)$$

presents the desired characteristics.

4.3.2. Extended Kalman filter

The only measurable state variable is the reactor temperature. The first step is to check the system observability. During step 1, all the state variables are observable. During step 2, the monomer concentration and number of particles are not observable, and during step 3, the number of particles is not observable. These variables are only predicted in these cases. The moments of the molecular weight are not observable and will be predicted only as in Schuler and Suzhen [52].

5. Experimental facilities

A schematic diagram of the experimental set-up is shown on Fig. 4.

The ingredients required to carry out the emulsion polymerization are

- the monomers (20% in mass): styrene and α-methylstyrene,
- deionized water,
- the emulsifier: here a mixture of Texapon NSO and Genapol PF20S ($G/T = 2$) at a concentration corresponding to 3 c.m.c. (critical micellar concentration),
- the initiator: potassium persulfate (1 g l^{-1}).

The reaction takes place in a 1 l glass tank reactor equipped with a stirrer, a reflux condenser, a sampling device and an inlet system for nitrogen. This reactor is heated or cooled with water which flows in a double jacket.

During the reaction, samples are withdrawn at suitable time intervals and the polymerization reaction is quenched with hydroquinone. Analysis of these samples is carried out off-line.

The conversion rate is determined by gravimetry (the conversion is calculated from the dry weight of the samples). The mean particle diameter is measured by dynamic light scattering (Malvern 4700). The number of particles is calculated from the conversion and particle size values. The molecular weight distribution is determined by size exclusion chromatography (linear Ultra Styragel columns) coupled with multi-angle laser light scattering (Dawn DSP-F, Wyatt Technology) and differential refractometry (Waters 410, Millipore).

The temperature control is achieved through a cooling fluid flowing in the double jacket at a constant flowrate. The cooling fluid inlet temperature is controlled using a three-way valve. The valve divides the outlet flow of the jacket into two streams. One of these streams is sent to a cold heat exchanger, the other one to a hot heat exchanger. The two exchangers outlets are then mixed again and returned back to the jacket.

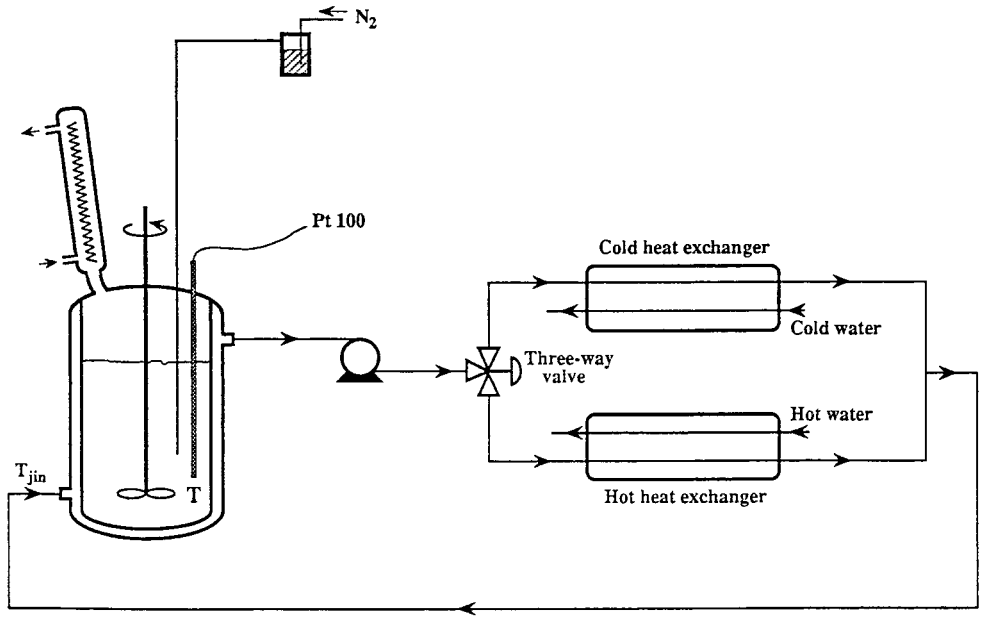

Fig. 4. Experimental rig.

Control and suitable measurements are realized with a micro-computer equipped with a data acquisition card with a sampling period of 10 s.

6. Experimental validation

The off-line computed optimal temperature profile is tracked experimentally with the non-linear geometric control law as described previously.

The results of two different experiments for two optimal profiles corresponding respectively to $X_f = 60\%$, $M_{nf} = 1.5\times10^6$ (exp. 1) and 2×10^6 g mol^{-1} (exp. 2) and a maximum reactor cooling rate of -0.04 K s^{-1} are presented.

Figs. 5 and 6 show the setpoint and measured reactor temperature. A very good setpoint temperature tracking is observed. The slight deviation at the beginning of the reaction can be explained by the initiator addition which creates a disturbance, then the trajectory is followed nearly without any oscillation.

The polymer quality is estimated by the extended Kalman filter from only temperature measurements, and then the estimations rely only upon the model accuracy. The estimations can be compared to the off-line measurements. Figs. 7 and 8 show that the experimental and estimated conversion

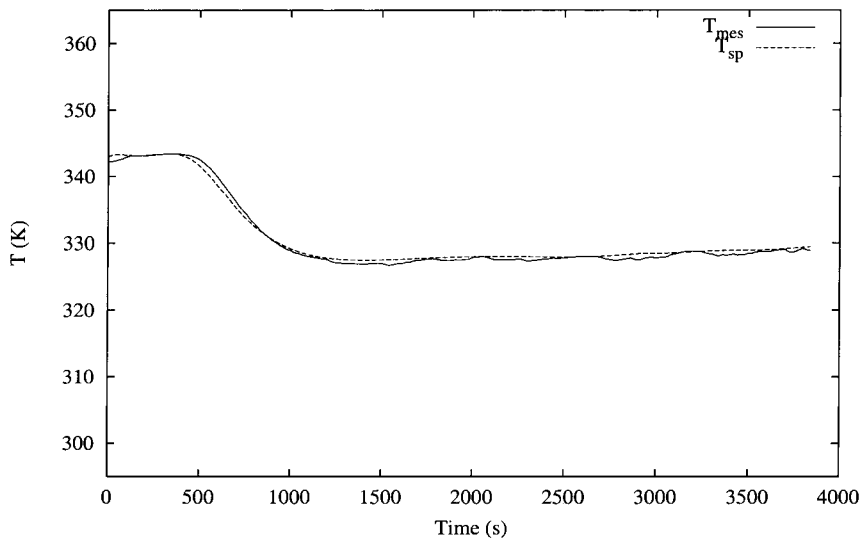

Fig. 5. Comparison between setpoint and measured temperature profiles – exp. 1.

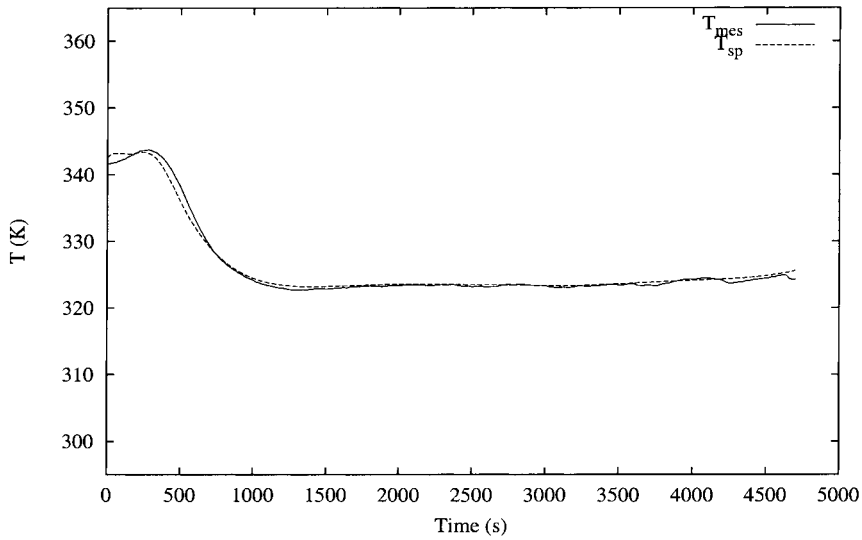

Fig. 6. Comparison between setpoint and measured temperature profiles – exp. 2.

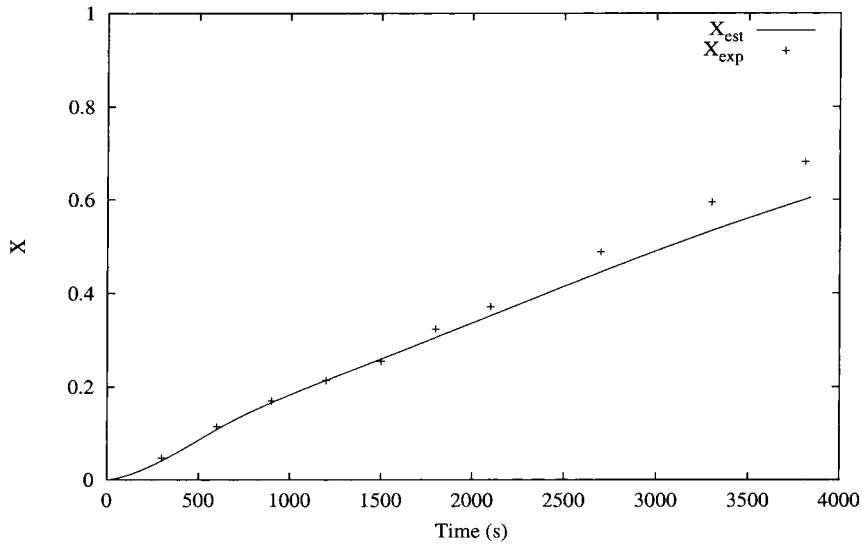

Fig. 7. Comparison between estimated and measured conversions – exp. 1.

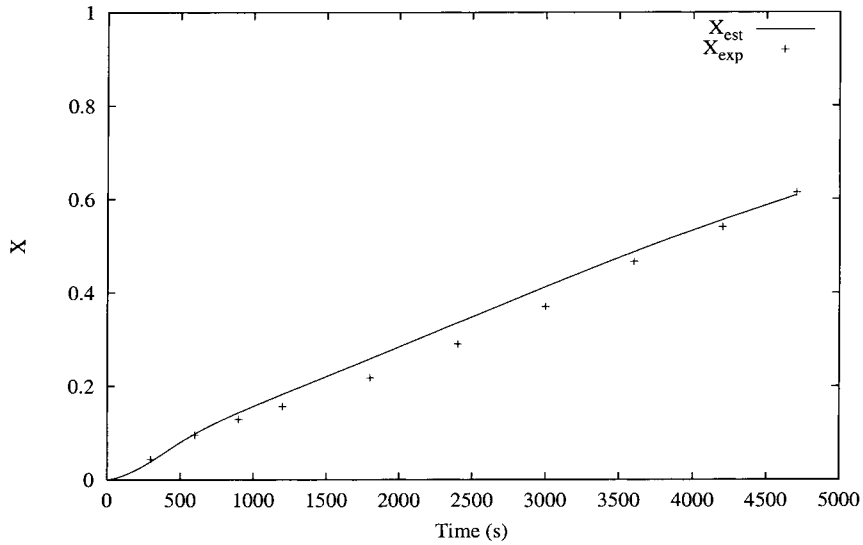

Fig. 8. Comparison between estimated and measured conversions – exp. 2.

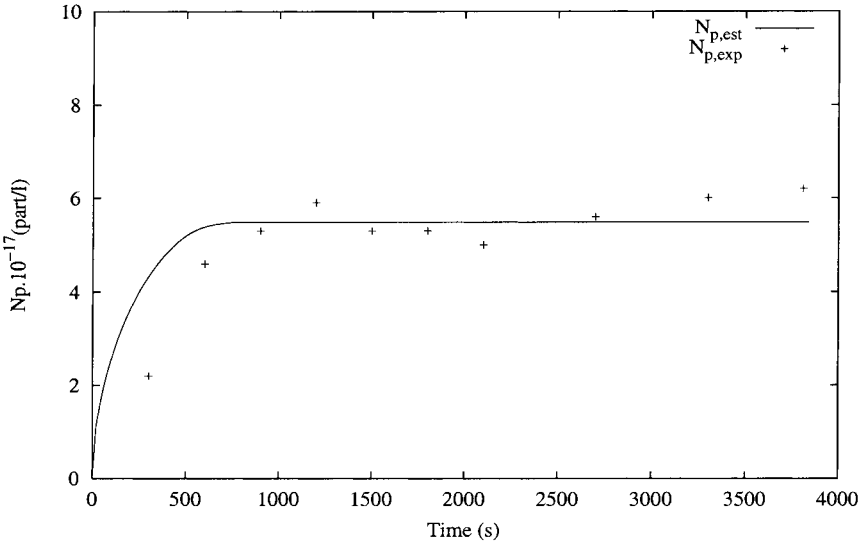

Fig. 9. Comparison between estimated and measured number of particles – exp. 1.

values for the same experiments are in good agreement. The first conversion profile leads to a final experimental conversion higher than the final predicted value whereas the second conversion profile is very close to the estimation. Figs. 9 and 10 present the experimental and estimated number of particles per volume unit. Despite the experimental errors in the determination of the number of particles, the agreement is quite satisfactory in both cases. In Figs. 11 and 12, the experimental and estimated number average molecular weight values are shown to be in very good agreement.

It must be underlined that the general agreement between experience and prediction observed is very satisfactory despite the experimental errors often involved in the polymer quality determinations such as the number of particles and the average molecular weight, and with only temperature measurements.

7. Conclusions

The optimal temperature profile for a complex polymerization reaction was determined. The objective was the minimization of the reaction time, while imposing constraints on the polymer quality. The optimization technique used, i.e. orthogonal collocation followed by sequential quadratic programming, is easy to implement, rapid and allows to take into account every kind of constraint, even

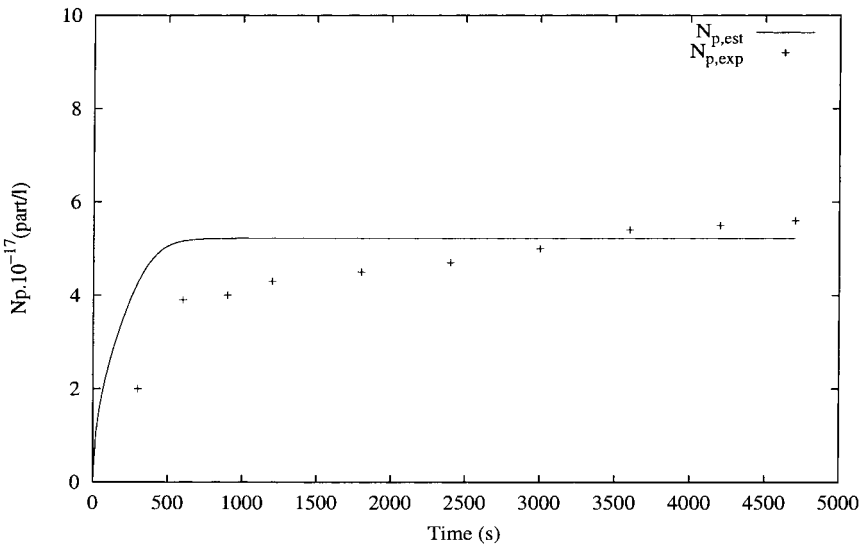

Fig. 10. Comparison between estimated and measured number of particles – exp. 2.

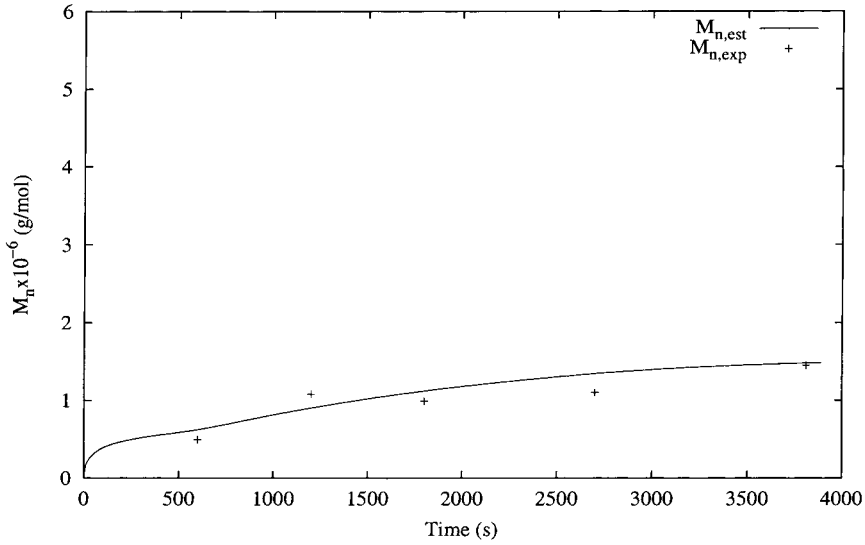

Fig. 11. Comparison between estimated and measured number average molecular weight - exp. 1.

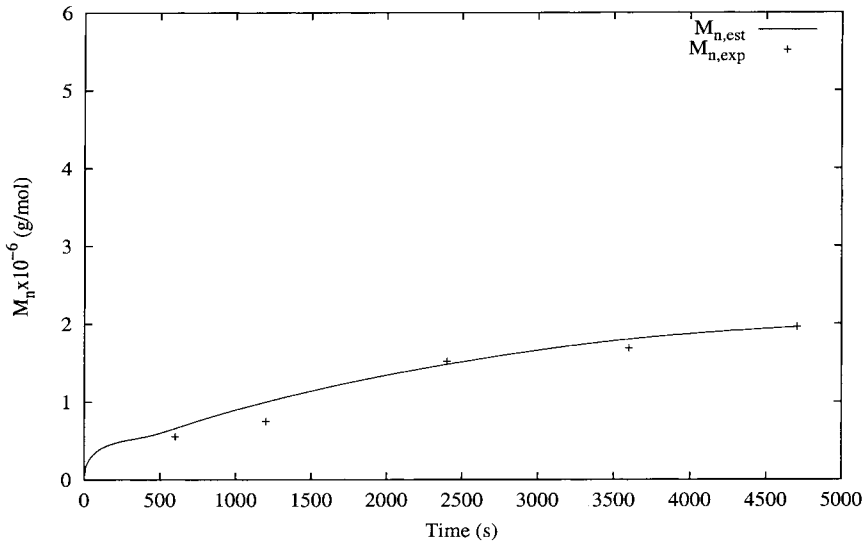

Fig. 12. Comparison between estimated and measured number average molecular weight – exp. 2.

more complex like constraints involving control variables time derivatives (corresponding to cooling limitations of the reactor used here). Non-linear geometric control allowed to track the rapid setpoint temperature decrease. An extended Kalman filter gave on-line good estimations of all state-variables and allowed to predict the macromolecular characteristics of the copolymer. The experimental validation gave very satisfactory results: the expected conversions and molecular weights were obtained.

8. Nomenclature

A	initiator concentration (mol l^{-1})/cooling surface (m^2)
a_s	surface area occupied by an emulsifier molecule (dm^2)
C_j	cooling fluid heat capacity (J kg^{-1} K^{-1})
f	initiator efficiency
F_j	cooling fluid flowrate (l s^{-1})
f_{MS}	α-methylstyrene molar fraction in the initial load
I_p	polydispersity index
k_{cm}	rate constant of initiator radical entry into micelles (l micelle^{-1} s^{-1})
k_{cp}	rate constant of initiator radical entry into particles (l part^{-1} s^{-1})
k_d	rate constant of initiator decomposition (s^{-1})
k_p	rate constant of propagation (l mol^{-1} s^{-1})
k_{trM}	rate constant of transfer to monomer (l mol^{-1} s^{-1})
L	kinetic chain length (g mol^{-1})

m number of micelles per volume unit (micelle l^{-1})
M global monomer concentration (mol l^{-1})
$m_r C_p$ reactor total heat capacity (J K^{-1})
M_M monomer molecular weight (g mol^{-1})
$\overline{M}_n$ number average molecular weight (g mol^{-1})
M_p monomer concentration in particles (mol l^{-1})
$\overline{M}_w$ weight average molecular weight (g mol^{-1})
$\overline{n}$ average radical number per particle
N number of inactive particles per volume unit (part l^{-1})
$N^{\cdot}$ number of active particles per volume unit (part l^{-1})
N_p total number of particles per volume unit (part l^{-1})
n_s aggregation number of micelles
P dead polymer concentration (mol l^{-1})
Q_i ith moment of the molecular weight distribution
$R^{\cdot}$ initiator radical concentration (mol l^{-1})
R_a initiator decomposition rate (mol l^{-1} s^{-1})
R_{cmax} maximal cooling rate of the reactor (K s^{-1})
R_p polymerization rate (mol l^{-1} s^{-1})
R_t termination rate (mol l^{-1} s^{-1})
R_{trM} transfer to monomer rate (mol l^{-1} s^{-1})
S emulsifier concentration (mol l^{-1})
T reactor temperature (K)
T_j jacket temperature (K)
T_{jin} cooling fluid inlet temperature (K)
U heat transfer coefficient (J K^{-1} s^{-1} m^{-2})
V reactor contents volume (l)
V_j reactor jacket volume (l)
X conversion rate
X_c critical conversion

Greek symbols

ΔH polymerization reaction enthalpy (J mol^{-1})
ε constant relative to the efficiency of the particles relative to the micelles in collecting an initiator radical
ρ_p polymer particle density (g l^{-1})
ρ_j cooling fluid density (g l^{-1})
ρ_M monomer density (g l^{-1})
ρ_P polymer density (g l^{-1})
ω_P polymer weight fraction in particles

Subscripts

est estimated
exp experimental
mes measured
sp setpoint
0 initial conditions

Supercripts

c computed
s specified

Acknowledgements

Authors are grateful to the 'Ministère de l'Education Nationale, de l'Enseignement Supérieur et de la Recherche' for its financial support.

References

[1] D. Tieu, W.R. Cluett, A. Penlidis, Polym. React. Eng. 2 (1994) 275.
[2] S.A. Chen, W.F. Jeng, Chem. Eng. Sci. 33 (1978) 735.
[3] S.A. Chen, K.F. Lin, Chem. Eng. Sci. 35 (1980) 2325.
[4] S.A. Chen, N.W. Huang, Chem. Eng. Sci. 36 (1981) 1295.
[5] G.Z.A. Wu, L.A. Denton, R.L. Laurence, Polym. Eng. Sci. 22 (1982) 1.
[6] I.M. Thomas, C. Kiparissides, Can. J. Chem. Eng. 62 (1984) 284.
[7] S.A. Chen, S.T. Lee, Polym. Eng. Sci. 25 (1985) 987.
[8] S.A. Chen, S.T. Lee, Polym. Eng. Sci. 27 (1987) 573.
[9] J.N. Farber, R.L. Laurence, Chem. Eng. Commun. 46 (1986) 347.
[10] S.R. Ponnuswamy, S.L. Shah, C.A. Kiparissides, Ind. Eng. Chem. Res. 26 (1987) 2229.
[11] K.Y. Hsu, S.A. Chen, Polym. Proc. Eng. 5 (1987) 151.
[12] K.Y. Hsu, S.A. Chen, Chem. Eng. Sci. 43 (1988) 1311.
[13] Y.J. Huang, L.J. Lee, J. Appl. Polym. Sci. 39 (1990) 2353.
[14] K.F. O'Driscoll, S.R. Ponnuswamy, J. Appl. Polym. Sci. 39 (1990) 1299.
[15] N.R. Vaid, S.K. Gupta, Polym. Eng. Sci. 31 (1991) 1708.
[16] D. Butala, W.R. Liang, K.Y. Choi, J. Appl. Polym. Sci. 44 (1992) 1759.
[17] B.R. Louie, D.S. Soong, J. Appl. Polym. Sci. 30 (1985) 3707.
[18] B.R. Louie, D.S. Soong, J. Appl. Polym. Sci. 30 (1985) 3825.
[19] M. Soroush, C. Kravaris, AIChE J. 38 (1992) 1429.
[20] G. Maschio, T. Bello, C. Scali, Chem. Eng. Sci. 49 (1994) 5071.
[21] C. Scali, R. Ciari, T. Bello, G. Maschio, J. Appl. Polym. Sci. 55 (1995) 945.
[22] A.R. Secchi, E.L. Lima, J.C. Pinto, Polym. Eng. Sci. 30 (1990) 1209.
[23] J.S. Chang, J.L. Lai, Ind. Eng. Chem. Res. 31 (1992) 861.
[24] S.S. Jang, W.L. Yang, Chem. Eng. Sci. 44 (1989) 515.
[25] S.S. Jang, P.H. Lin, Chem. Eng. Sci. 46 (1991) 3153.
[26] L.T. Biegler, Comp. Chem. Eng. 8 (1984) 243.
[27] G. Arzamendi, J.M. Asua, J. Appl. Polym. Sci. 38 (1989) 2019.
[28] G. Arzamendi, J.M. Asua, Ind. Eng. Chem. Res. 30 (1991) 1342.
[29] J.R. Leiza, G. Arzamendi, J.M. Asua, Polym. Int. 30 (1993) 455.
[30] J.C. de La Cal, A. Echevarria, G.R. Meira, J.M. Asua, J. Appl. Polym. Sci. 57 (1995) 1063.
[31] A. Rudin, M.C. Samanta, J. Appl. Polym. Sci. 24 (1979) 1665.
[32] R.E. Branton, H.P. Plaumann, J.J. Sendorek, J. Appl. Polym. Sci. 40 (1990) 1149.
[33] J.R. Castellanos, Contribution à la modélisation du procédé de copolymérisation en émulsion de l'α-méthylstyrène et du styrène, Ph.D. Thesis, I.N.P.L., 1996.
[34] J.M. Asua, M.E. Adams, E.D. Sudol, J. Appl. Polym. Sci. 39 (1990) 1183.
[35] H. Gerrens, Zeitschrift für Elektrochemie 60 (1956) 400.
[36] M. Harada, M. Nomura, H. Kojima, W. Eguchi, S. Nagata, J. Appl. Polym. Sci. 16 (1972) 811.
[37] J. Villermaux, L. Blavier, Chem. Eng. Sci. 39 (1984) 87.
[38] J.E. Cuthrell, L.T. Biegler, AIChE J. 33 (1987) 1257.
[39] J.G. Renfro, A.M. Morshedi, O.A. Asbjornsen, Comp. Chem. Eng. 11 (1987) 503.
[40] J.Y. Lin, Z.H. Yang, Int. J. Cont. 47 (1988) 1915.
[41] C.J. Goh, K.L. Teo, Automatica 24 (1988) 3.
[42] C.T. Chen, C. Hwang, Chem. Eng. Commun. 97 (1990) 9.
[43] C.P. Neuman, A. Sen, Automatica 9 (1973) 601.

[44] T.H. Tsang, D.M. Himmelblau, T.F. Edgar, Int. J. Control 21 (1975) 763.
[45] J.E. Cuthrell, L.T. Biegler, Comp. Chem. Eng. 13 (1989) 49.
[46] D. Tieu, W.R. Cluett, A. Penlidis, Comp. Chem. Eng. 19 (1995) 375.
[47] K. Schittkowski, Ann. Oper. Res. 5 (1985) 485.
[48] A. Isidori, Non-linear Control Systems: An Introduction, Springer-verlag, New York, 1995.
[49] J. Alvarez, R. Suarez, A. Sanchez, Chem. Eng. Sci. 49 (1994) 3617.
[50] Z.L. Wang, J.P. Corriou, F. Pla, Comp. Chem. Eng. 18 (1994) S397.
[51] K. Watanabe, Adaptive Estimation and Control, Prentice Hall, London, 1992.
[52] H.R. Schuler, Z. Suzhen, Chem. Eng. Sci. 40 (1985) 1891.